Research Article

Outage Performance Analysis of STAR-RIS-NOMA Networks under Imperfect CSI

Sang Quang NGUYEN[1], *Anh-Tu LE*[2], *Van-Duc PHAN*[3], *Huynh Thanh THIEN*[4,*], *Rupak KHAREL*[5]

[1]Posts and Telecommunications Institute of Technology Ho Chi Minh City, Vietnam
[2]Science and Technology Application for Sustainable Development Research Group, Ho Chi Minh City University of Transport, Ho Chi Minh City, Vietnam.
[3]Faculty of Automotive Engineering, School of Technology, Van Lang University, Ho Chi Minh City, Vietnam.
[4]Faculty of Electrical and Electronics Engineering, Ton Duc Thang University, Ho Chi Minh City, Vietnam.
[5]School of Computing and Engineering, University of Huddersfield, Huddersfield HD1 3DH, United Kingdom.

sangnqdv05@gmail.com, tula@ut.edu.vn, duc.pv@vlu.edu.vn, huynhthanhthien@tdtu.edu.vn, r.kharel@hud.ac.uk.

*Corresponding author: Huynh Thanh Thien; huynhthanhthien@tdtu.edu.vn

DOI: 10.15598/aeee.v22i3.5546

Article history: Received Nov 10, 2023; Revised Jul 02, 2024; Accepted Aug 01, 2024; Published Sep 30, 2024.

Abstract. *In this paper, we investigate the performance of simultaneously transmitting and reflecting reconfigurable intelligent surfaces (STAR-RISs)-assisted non-orthogonal multiple access (NOMA) networks under imperfect channel state information (CSI). Furthermore, we derive the exact analytical equations for the OP of two users. To obtain insight into the high power domain, the asymptotic analysis outage probability (OP) is studied. Further, the Monte-Carlo methods verified the tightness of all derivations. Finally, the results indicate that when increasing the number of elements of STAR-RIS, the STAR-RIS-NOMA networks can achieve improved outage performance.*

Keywords

STAR-RIS, NOMA, imperfect channel state information, outage probability.

1. Introduction

The requirement for high-data-rate and low-latency wireless transmission technologies will grow rapidly in the next sixth-generation (6G) era, making new wireless transmission technologies increasingly critical [1–4]. Additionally, the authors in [5–8] used the relay to increase the incident signal's dispersion. Different from relay, by adjusting the phase and amplitude of each element, reconfigurable intelligent surfaces (RISs), a promising technology based on numerous reconfigurable passive elements, can improve the propagation of the incident signal to improve the quality of the environment [9–13]. However, RIS that simply reflects light can cover the front side of a surface. Recently, the idea of simultaneously transmitting and reflecting-RIS (STAR-RIS) was introduced in [14] and [15] to solve the constraints of RIS. The operation of STAR-RIS is based on the electromagnetic wave phenomena of reflection and refraction. The STAR-RIS system is constructed such that when radio waves are received, time-varying electric and magnetic fields are activated [16]. On either side of the STAR-RIS, these time-varying fields have the ability to transmit and reflect.

High spectrum efficiency and extensive connection are further benefits of non-orthogonal multiple access (NOMA) technology [17–19]. Since numerous customers may be supplied at the same time, frequency, and code resource thanks to power domain multiplexing at the transmitter, NOMA is particularly capable of outperforming traditional orthogonal multiple access (OMA) approaches [20]. Therefore, NOMA is viewed as a potential solution for mobile networks with limited resource availability in the future. The combination of the two procedures would present a win-win alternative given the attractive qualities of RIS and NOMA [21].

The effectiveness of STAR-RIS across fading channels was previously investigated in [22–27]. An ergodic rate analysis of a NOMA system with STAR-RIS executing the ES protocol over Nakagami-m fading channels was the main topic of the work published in [22]. Since the investigation focused on mobile phone users without a line-of-sight (LoS) connection to the base station (BS), it was demonstrated that STAR-RIS performs better than traditional RIS in NOMA systems. Additionally, the authors of [23] provided statistical channel state information (CSI) and contrasted the outcomes of using MS and ES procedures. In [24], it was shown that the performance of STAR-RIS-aided NOMA without a direct connection from the BS to users might be adjusted out by inversely unequal resource distribution at STAR-RIS in low SNR zones. The ergodic rate and outage probability of STAR-RIS aided NOMA systems were calculated in [25]. By dividing the STAR-RIS surface, the two-user NOMA system was upgraded to a multi-user system [26]. Additionally, in order to assess the effects of channel correlations, the outage probability of systems across spatially correlated channels was also explored in [27]. Based on these advances in STAR-RIS-NOMA networks, in this paper, we investigated the performance of STAR-RIS-NOMA networks with randomly deployed users and the impact of imperfect CSI (ipCSI). Furthermore, we derived the accurate analytical formulations of outage probability (OP) for two users. In addition, the asymptotic OP is investigated to obtain the insight of the proposed system. Finally, all derivations are validated using the Monte Carlo method. Table 1 summarizes the comparative novelty of our article with the existing studies.

The remainder of the paper is structured as follows. The system model is introduced in Section 2. . Section 3. investigates the system's outage performance. In Section 4. , we calculate the asymptotic outage probability for two users and find diversity orders at high SNR. Section 5. includes simulation to validate the conclusions from Section 3. . Section 6. is the conclusion.

2. System Model

We explore a STAR-RIS-based NOMA system with a source (S), randomly placed users, and a STAR-RIS at a cell-edge area where the transmission lines from the S to the users are non-line-of-sight (NLoS). As illustrated in Fig. 1, the channel is denoted by $h_{0,n}$ for the link from the S to the STAR-RIS, $h_{1,n}$ near user (U_1) and $h_{2,n}$ far user (U_2) for the links from the STAR-RIS to the reflecting and refracting users, respectively. We

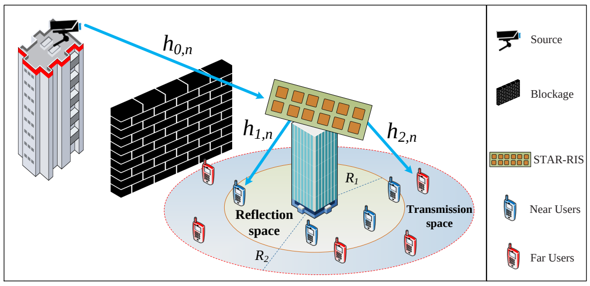

Fig. 1: Illustration of STAR-RIS-aided NOMA network model.

assume that there are no direct linkages between the S and two users. This might be due to impediments, an urgent obstruction, or other factors. The following sections show detailed system model designs. obstacles, urgent disasters and so forth.

2.1. Deployment

The S is fixed, as indicated in Fig. 1 and direct linkages from the S to users are prevented. We suppose that the users are in a circle and that the STAR-RIS is in the middle. The far field is assumed because the distance between the S and the users is substantially greater than the top bound of the near field. To test the performance of users at various distances from the STAR-RIS, the users are divided into two groups: close users deployed in the inner circle with a radius R_1 meters and distant users placed in the outer ring with radii R_2 and R_1 meters. To simulate the user locations, we employ homogeneous poisson point processes [32, 33]. As a result, the near and far users are distributed evenly inside their regions, and the probability density functions (PDFs) of the distances from a user to the center are generated as The S is fixed, as indicated in Fig. 1 and direct linkages from the S to users are prevented. We suppose that the users are in a circle and that the STAR-RIS is in the middle. The far field is assumed because the distance between the S and the users is substantially greater than the top bound of the near field. To test the performance of users at various distances from the STAR-RIS, the users are divided into two groups: close users deployed in the inner circle with a radius R_1 meters and distant users placed in the outer ring with radii R_2 and R_1 meters. To simulate the user locations, we employ homogeneous poisson point processes [32, 33]. As a result, the near and far users are distributed evenly inside their regions, and PDFs of the distances from a user to the center are generated as [43]. The S is fixed, as indicated in Fig. 1 and direct linkages from the S to users are prevented. We suppose that the users are in a circle and that the STAR-RIS is in the middle. The far field is assumed because the distance between the S and the users is substantially greater than the top bound of the near field. To test

Tab. 1: Comparison between the novelty of our work and previous papers.

Ref./Prop.	STAR-RIS	NOMA	Imperfect CSI	Randomly Placed users	OP Expression
[28]	X	✓	X	X	✓
[29]	✓	✓	X	X	✓
[30]	✓	✓	X	X	✓
[31]	✓	✓	✓	X	X
Our study	✓	✓	✓	✓	✓

the performance of users at various distances from the STAR-RIS, the users are divided into two groups: close users located in the inner circle with a radius R_1 meters and distant users placed in the outer ring with radii R_2 and R_1 meters. To simulate the user locations, we employ homogeneous poisson point processes [32,33]. As a result, the near and far users are distributed evenly inside their regions, and PDFs of the distances from a user to the center are generated as [34]

$$f_{d_D}(x) = \frac{\partial}{\partial x}\frac{\pi x^2}{\pi R_1^2} = \frac{2x}{R_1^2}, \tag{1a}$$

$$f_{d_E}(x) = \frac{\partial}{\partial x}\frac{\pi\left(x^2 - R_1^2\right)}{\pi\left(R_2^2 - R_1^2\right)} = \frac{2x}{R_2^2 - R_1^2}. \tag{1b}$$

2.2. STAR-RIS Assisted downlink Model

To maximize the gain for each user while considering unicast transmission, we assume that a NOMA pair consists of a near user and a far user on opposite sides of the STAR-RIS. When average performance is considered, near users have greater channel quality than far users. The S will allocate more energy to distant consumers than to close users. As a result, the close users will employ the SIC procedure, while the remote users will decode their signals directly. The power allocation coefficients are denoted as $a_2 > a_1$ with $a_2 + a_1 = 1$. Furthermore, the channel for LoS can be modeled as Nakagami-m fading [36] and nLoS can be modeled by Rayleigh fading [37,38]. Thus, we assume all the channels follow independent Rayleigh fading for nLoS in this paper. Then, the received signals at two users are expressed by

$$\bar{y}_{U_i} = \frac{\left(\sqrt{a_1 P_S}\bar{x}_1 + \sqrt{a_1 P_S}\bar{x}_2\right)}{\sqrt{d_0^\alpha d_{U_i}^\alpha}} \times \left(\sum_{n=1}^{N} h_{0,n}h_{i,n}\varepsilon_n^{U_i} + \bar{e}_{U_i}\right) + \bar{\omega}_{U_i}, \quad i \in \{1,2\} \tag{2}$$

where P_S is the power at S, $\bar{x}_i$ is the unit-power signal for U_i, $\bar{\omega}_{U_i}$ is the additive white Gaussian noise (AWGN) with $\bar{\omega}_{U_i} \sim \mathcal{CN}\left(0, \sigma_{U_1}^2\right)$, d_0 is the distance between the S and the STAR-RIS, and d_{U_i} is the distance between the STAR-RIS and two users. Furthermore, α serves as the pass-loss exponent, $\varepsilon_n^{U_i} = \beta_{U_i}e^{j\phi_{U_i}}$ is the response of the two users, while ϕ_{U_i} and β_{U_i} indicate the reflection coefficients of phase shift and amplitude of U_i. We assume $\beta_{U_i} = 1$ without losing generality. Moreover, $\bar{e}_{U_i}$ denotes the channel estimation error, which may be represented as a complex Gaussian random variable (CGRV) with $\bar{e}_{U_i} \sim \mathcal{CN}\left(0, \sigma_{e_i}^2\right)$ and $\sigma_{e_i}^2 = \delta^2\left\|vec\left(\sum_{n=1}^{N} h_{0,n}h_{i,n}\varepsilon_n^{U_i}\right)\right\|_2^2$, $\delta \in [0,1)$ which represents the proportion of channel status information (CSI) uncertainties.

We concentrate on error transmission performance, therefore we assume that STAR-RIS is fully aware of phase $\phi_{h_{0,n}}$ of the S to STAR-RIS channel $h_{0,n}$ and phase $\phi_{h_{i,n}}$ of the STAR-RIS to U_i channel $h_{i,n}$, and select the optimal phase shift, i.e. $\phi_{U_i} = -\left(\phi_{h_{0,n}} + \phi_{h_{i,n}}\right)$.

The received signal of U_i may be rewritten as

$$\bar{y}_{U_i} = \underbrace{\left(\sqrt{d_0^\alpha d_i^\alpha}\right)^{-1} A_i \sum_{q=1}^{2}\sqrt{a_q P_S}\bar{x}_q}_{\text{desired information signal}} + \underbrace{\bar{\omega}_{U_i}}_{\text{AWGN}} + \underbrace{\left(\sqrt{d_0^\alpha d_i^\alpha}\right)^{-1}\bar{e}_{U_i}\sum_{q=1}^{2}\sqrt{a_q P_S}\bar{x}_q}_{\text{ipCSI noise}}, \tag{3}$$

where $A_1 = \sum_{n=1}^{N}|h_{0,n}||h_{1,n}|$ and $A_2 = \sum_{n=1}^{N}|h_{0,n}||h_{2,n}|$ are the estimated channel coefficient.

From (3), since the NOMA scheme is adopted, i.e. U_1 first decodes the information intended for x_2 of U_2, by treating x_1 as the interference signal (IS). Hence, the received signal-to-interference-plus-noise ratio (SINR) at U_1 to detect x_2 is given by

$$\gamma_{U_1,x_2} = \frac{a_2 P_S (d_0^\alpha d_i^\alpha)^{-1}|A_1|^2}{a_1 P_S (d_0^\alpha d_i^\alpha)^{-1}|A_1|^2 + (d_0^\alpha d_i^\alpha)^{-1} P_S \sigma_{e_1}^2 + \sigma_{U_1}^2}. \tag{4}$$

We can rewrite SINR at user U_1 as below

$$\gamma_{U_1,x_2} = \frac{a_2\rho_S|A_1|^2}{a_1\rho_S|A_1|^2 + \rho_S\sigma_{e_1}^2 + d_0^\alpha d_1^\alpha}, \tag{5}$$

We assume $\sigma_U^2 = \sigma_{U_1}^2 = \sigma_{U_2}^2$ then $\rho_S = P_S/\sigma_U^2$ denotes the transmit signal-to-noise radio (SNR) at S. Next, we assume perfect SIC then the SINR at U_1 to detect its own signal x_1 is given as

$$\gamma_{U_1,x_1} = \frac{a_1\rho_S|A_1|^2}{\rho_S\sigma_{e_1}^2 + d_0^\alpha d_1^\alpha}. \tag{6}$$

Given (3), U_2 detects the designated signal $\tilde{x}_2$, treating $\tilde{x}_1$ as interference. The instantaneous SINR at U_2 from

$$\gamma_{U_2} = \frac{a_2\rho_S|A_2|^2}{a_1\rho_S|A_2|^2 + \rho_S\sigma_{e_2}^2 + d_0^\alpha d_2^\alpha}. \tag{7}$$

3. Outage Probability Analysis

First, we examine performance indicators in the STAR-RIS-assisted NOMA system, namely the outage probability (OP). An approximation analysis is also provided to provide more insights.

3.1. Channel model

Based on [35], the PDF and CDF of the cascade channel gain of $|A_1|^2$ and $|A_2|^2$ as

$$f_{|A_1|^2}(x) = \frac{2x^{\frac{N-1}{2}}}{\Gamma(N)\left(\sqrt{\lambda_{h_0}\lambda_{h_1}}\right)^{N+1}} K_{N-1}\left(2\sqrt{\frac{x}{\lambda_{h_0}\lambda_{h_1}}}\right), \tag{8a}$$

$$f_{|A_2|^2}(x) = \frac{2x^{\frac{N-1}{2}}}{\Gamma(N)\left(\sqrt{\lambda_{h_0}\lambda_{h_2}}\right)^{N+1}} K_{N-1}\left(2\sqrt{\frac{x}{\lambda_{h_0}\lambda_{h_2}}}\right), \tag{8b}$$

and

$$F_{|A_1|^2}(x) = 1 - \frac{2x^{\frac{N}{2}}}{\Gamma(N)\left(\sqrt{\lambda_{h_0}\lambda_{h_1}}\right)^{N}} K_{N}\left(2\sqrt{\frac{x}{\lambda_{h_0}\lambda_{h_1}}}\right), \tag{9a}$$

$$F_{|A_2|^2}(x) = 1 - \frac{2x^{\frac{N}{2}}}{\Gamma(N)\left(\sqrt{\lambda_{h_0}\lambda_{h_2}}\right)^{N}} K_{N}\left(2\sqrt{\frac{x}{\lambda_{h_0}\lambda_{h_2}}}\right), \tag{9b}$$

where $K_v(.)$ and $\Gamma(.)$ are so-called the Bessel function and the Gamma function respectively [39].

3.2. Outage Probability of Near User

If near user U_1 fails to decode signal x_1 in the STAR-RIS NOMA protocol, this is referred to as an outage event. To effectively decode signal x_1, two requirements must be met: i) near user U_1 successfully decodes signal x_2; ii) near user U_1 successfully decodes its own signal x_1. Then, in the downlink phase, the outage probability of U_1 may be expressed as

$$\begin{aligned}\mathcal{O}_1 =& 1 - \Pr\left(\gamma_{U_1,x_2} > \varepsilon_2, \gamma_{U_1,x_1} > \varepsilon_1\right)\\ =& 1 - \Pr\left(\begin{array}{c}|A_1|^2 > \psi_2\left(\rho_S\sigma_{e_1}^2 + d_0^\alpha d_1^\alpha\right),\\ |A_1|^2 > \psi_1\left(\rho_S\sigma_{e_1}^2 + d_0^\alpha d_1^\alpha\right)\end{array}\right)\\ =& 1 - \Pr\left(|A_1|^2 > \psi_{\max}\left(\rho_S\sigma_{e_1}^2 + d_0^\alpha d_1^\alpha\right)\right),\end{aligned} \tag{10}$$

where $\varepsilon_i = 2^{R_{th,i}} - 1$, $i \in \{1,2\}$ with R_i being the target rate at U_i, $\psi_1 = \frac{\varepsilon_1}{a_1\rho_S}$, $\psi_2 = \frac{\varepsilon_2}{\rho_S(a_2 - \varepsilon_2 a_1)}$ and $\psi_{\max} = \max(\psi_1, \psi_2)$.

Theorem 1: The approximation OP of near user can be obtained as

$$\begin{aligned}\mathcal{O}_1 \approx& 1 - \frac{2\pi\psi_{\max}^{\frac{N}{2}}}{R_1 Q\Gamma(N)\left(\sqrt{\lambda_{h_0}\lambda_{h_1}}\right)^N}\sum_{q=1}^{Q}\sqrt{1-\phi_q^2}\\ &\times \Phi(\phi_q)\left(\rho_S\sigma_{e_1}^2 + d_0^\alpha\Phi(\phi_q)^\alpha\right)^{\frac{N}{2}}\\ &\times K_N\left(2\sqrt{\frac{\psi_{\max}\left(\rho_S\sigma_{e_1}^2 + d_0^\alpha\Phi(\phi_q)^\alpha\right)}{\lambda_{h_0}\lambda_{h_1}}}\right),\end{aligned} \tag{11}$$

where $\phi_q = \cos\left(\frac{2q-1}{2Q}\pi\right)$.

Proof: See Appendix A

3.3. Outage Probability of Far User

The outage probability of user U_2 is required to analyze the performance of such a system in meeting the specific requirement of target rates. It is easier to achieve an outage probability for user U_2 since it just needs to decode its own information.

According to the NOMA protocol, the outage events of user U_2 occurs when it cannot decode message x_2 successfully

$$\begin{aligned}\mathcal{O}_2 &= 1 - \Pr\left(\gamma_{U_2} > \varepsilon_2\right)\\ &= \begin{cases}1 - \Pr\left(|A_2|^2 > \dfrac{\left(\rho_S\sigma_{e_2}^2 + d_0^\alpha d_2^\alpha\right)}{\psi_2^{-1}}\right) & , if\ a_2 > \varepsilon_2 a_1\\ 1 & , if\ a_2 < \varepsilon_2 a_1\end{cases}\end{aligned} \tag{12}$$

Theorem 2: The approximation OP of far user can be obtained by

$$\begin{aligned}\mathcal{O}_2 \approx & 1 - \frac{2\pi\left(R_2 - R_1\right)\psi_2^{\frac{N}{2}}}{Q\left(R_2^2 - R_1^2\right)\Gamma\left(N\right)\left(\sqrt{\lambda_{h_0}\lambda_{h_2}}\right)^N} \\ & \times \sum_{q=1}^{Q}\sqrt{1-\phi_q^2}\Delta\left(\phi_q\right)\left(\rho_S\sigma_{e_2}^2 + d_0^\alpha\Delta(\phi_q)^\alpha\right)^{\frac{N}{2}} \\ & \times K_N\left(2\sqrt{\frac{\psi_2\left(\rho_S\sigma_{e_2}^2 + d_0^\alpha\Delta(\phi_q)^\alpha\right)}{\lambda_{h_0}\lambda_{h_2}}}\right)dt. \end{aligned} \tag{13}$$

Proof: See Appendix B

4. Asymptotic Computation of The Main Performance Metric

We examine the asymptotic expressions in order to gain more insight a the very high power domain. Considering the analytical findings in (18) and (12), when $\rho \to \infty$, the asymptotic expression for $\mathcal{O}_1^\infty = 1 - \Pr\left(\gamma_{U_1,x_2}^\infty > \varepsilon_2, \gamma_{U_1,x_1}^\infty > \varepsilon_1\right)$ and $\mathcal{O}_2^\infty = 1 - \Pr\left(\gamma_{U_2}^\infty > \varepsilon_2\right)$ with $\gamma_{U_1,x_2}^\infty = \frac{a_2|A_1|^2}{a_1|A_1|^2+\sigma_{e_1}^2}$, $\gamma_{U_1,x_1}^\infty = \frac{a_1|A_1|^2}{\sigma_{e_1}^2}$ and $\gamma_{U_2}^\infty = \frac{a_2|A_2|^2}{a_1|A_2|^2+\sigma_{e_2}^2}$ are given as

$$\begin{aligned}\mathcal{O}_1^\infty = & 1 - \Pr\left(\gamma_{U_1,x_2}^\infty > \varepsilon_2, \gamma_{U_1,x_1}^\infty > \varepsilon_1\right) \\ = & 1 - \Pr\left(\left|A_1\right|^2 > \theta_2, \left|A_1\right|^2 > \theta_1\right) \\ = & 1 - \Pr\left(\left|A_1\right|^2 > \theta_{\max}\right) \\ = & F_{|A_1|^2}\left(\theta_{\max}\right), \end{aligned} \tag{14}$$

and

$$\begin{aligned}\mathcal{O}_2^\infty = & 1 - \Pr\left(\gamma_{U_2}^\infty > \varepsilon_2\right) \\ = & 1 - \Pr\left(\left|A_2\right|^2 > \frac{\varepsilon_2\sigma_{e_2}^2}{a_2 - \varepsilon_2 a_1}\right) \\ = & F_{|A_2|^2}\left(\frac{\varepsilon_2\sigma_{e_2}^2}{a_2 - \varepsilon_2 a_1}\right). \end{aligned} \tag{15}$$

where $\theta_1 = \frac{\varepsilon_1\sigma_{e_1}^2}{a_1}$, $\theta_2 = \frac{\varepsilon_2\sigma_{e_1}^2}{a_2-\varepsilon_2 a_1}$ and $\theta_{\max} = \max\left(\theta_1, \theta_2\right)$.

Substituting (9a) into (14) and (9b) into (15), the asymptotic expressions for outage probability of U_1 and U_2 for STAR-RIS NOMA networks can be respectively given by

$$\mathcal{O}_1^\infty = 1 - \frac{2\theta_{\max}^{\frac{N}{2}}}{\Gamma\left(N\right)\left(\sqrt{\lambda_{h_0}\lambda_{h_1}}\right)^N}K_N\left(2\sqrt{\frac{\theta_{\max}}{\lambda_{h_0}\lambda_{h_1}}}\right), \tag{16}$$

and

$$\begin{aligned}\mathcal{O}_2^\infty = & 1 - \frac{2}{\Gamma\left(N\right)\left(\sqrt{\lambda_{h_0}\lambda_{h_2}}\right)^N}\left(\frac{\varepsilon_2\sigma_{e_2}^2}{a_2 - \varepsilon_2 a_1}\right)^{\frac{N}{2}} \\ & \times K_N\left(2\sqrt{\frac{\varepsilon_2\sigma_{e_2}^2}{\lambda_{h_0}\lambda_{h_2}\left(a_2 - \varepsilon_2 a_1\right)}}\right). \end{aligned} \tag{17}$$

Remark: *From the definition of the diversity order, which is defined as [40, 41]* $d_i = -\lim_{\rho_S\to\infty}\frac{\log(\mathcal{O}_i^\infty)}{\log(\rho_S)}$, $i \in \{1, 2\}$. *Based on the analytical conclusion in* (16) *and* (17)*, the asymptotic outage probability of* U_1 *and* U_2 *for imperfect CSI may be determined by using a high SNR regime, that is, when* ρ_S *approaches infinity. As a result, with incomplete CSI, the diversity orders of* d_1 *and* d_2 *are equal to zero.*

5. Results and Discussion

In this section, we assess the performance of the derived theoretical expression. Numerical results are also produced in order to validate the provided analytical expression. In the following figures, we denote "Ana.", "Sim.", "Asymp." as analytical computation, simulation, and asymptotic analysis, respectively, and the Monte Carlo approach is utilized to get simulation results as in [42–51]. The target rate is set to be $R_{th,1} = 2$, $R_{th,2} = 1$ bit per channel use (BPCU) for U_1 and U_2, respectively. In particular, the main parameters can be seen in Table 2. In addition, the equivalent noise power at D_1 and D_2 are $\omega_{U_1}^2 = \omega_{U_2}^2 = N_0 + 10\log\left(\text{BW}\right) + \text{NF}$ [dBm] in [52]. One of our code's technological contributions is that we employ symbolic calculations in Matlab to achieve very accurate results. In addition, the Gauss-Chebyshev parameter is selected as $Q = 100$ to yield a close approximation .

Tab. 2: Main system parameters

Monte Carlo simulations	10^7 iterations
Power allocation factors	$a_1 = 0.1$ & $a_2 = 0.9$
The radii of the inner	$R_1 = 20$ m
The radii of the outer	$R_2 = 50$ m
Total reflecting elements	$N = 16$
Bandwidth	BW = 10 MHz
Noise figure	NF = 10 dBm
Thermal noise power density	$N_0 = -174$ dBm/Hz
Distance from S to STAR-RIS	$d_0 = 20$ m
The path loss exponent	$\alpha = 3$
ipCSI impact factor	$\delta^2 = 0.01$

Fig 2 plots the OP versus P_S[dBm] with different the number of elements of STAR-RIS. The analytical

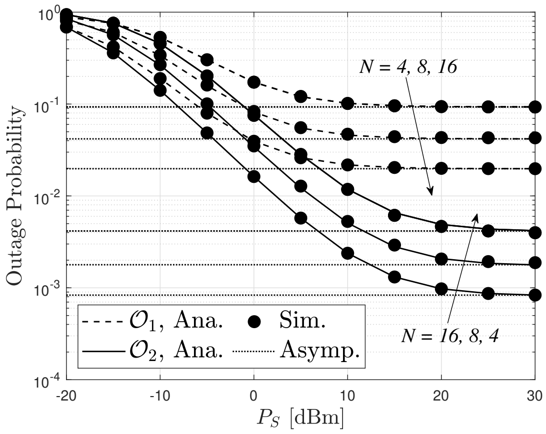

Fig. 2: Outage probability versus P_S, with $N = \{4, 8, 16\}$.

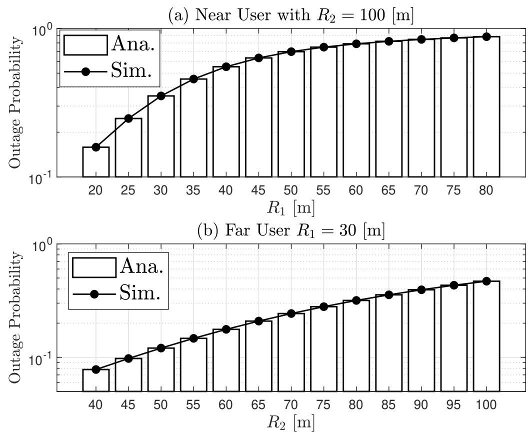

Fig. 3: Outage probability of the near users and far users versus the radius R_1 and R_2, respectively, with $P_S = -5$ [dBm] and $N = 8$.

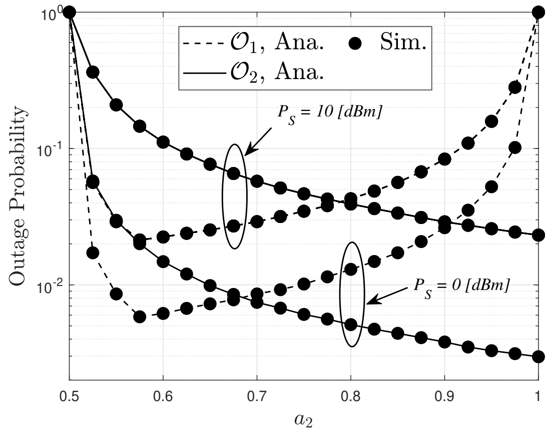

Fig. 4: Outage probability versus power allocation factor a_2, with $R_1 = 30$ m, $R_2 = 60$ m and $N = 16$.

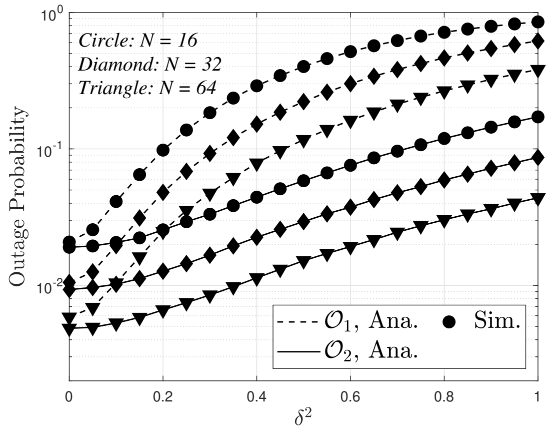

Fig. 5: Outage probability of STAR-RIS NOMA versus imperfect CSI, with $P_S = 5$ [dBm].

results for OP of U_1 and U_2 corresponding to the results derived in (11) and (13), respectively, match perfectly with Monte Carlo simulation results. In addition, the asymptotic results are plotted based on (16) and (17), respectively. As can be observed, the outage performance of U_1 and U_2 are improved when increasing the number of elements of STAR-RIS. In addition, the performance of the STAR-RIS-NOMA network works in low transmit SNR. In Fig 3, we plotted the OP of Near User and Far User versus the corresponding radius R_1 and R_2 respectively. As can be seen, the performance is increased in a low radius.

Fig 4 depicts the ideal outage probability of users D_1, D_2 at various times of a_2. These findings are explained by the fact that power allocation factors a_1 and a_2 contribute to the variance in SINR as well as the associated outage probability, with $a_1 = 0.575$ exhibiting optimal outage probability for D_1. These findings also show that changing the power has a small effect on outage probability, as evidenced by the two cases of P_s within the observed area. High transmit SNR at the S is intuitively thought to result in greater outage performance. Fig. 5 plotted the performance of U_1 and U_2 versus the impact of imperfect CSI. We can observe that the performance is better in the low impact of ipCSI.

Fig. 6 show the Outage probability versus P_S in dBm to compare between STAR-RIS-NOMA and STAR-RIS-OMA. It can be observed as the performance of STAR-RIS-NOMA is better than STAR-RIS-OMA. This can explain that in STAR-RIS-NOMA only one time slot is needed to transmit information. As for STAR-RIS-OMA, it needs to use two time slots to transmit information.

6. Conclusion

In this study, we investigated the performance of STAR-RIS-NOMA networks. Specifically, we have evaluated the outage performance of two users un-

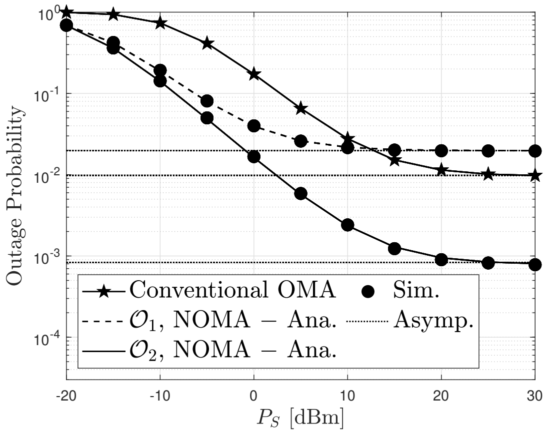

Fig. 6: Comparison between NOMA and OMA: Outage probability versus P_S in dBm, with $N = 16$.

der the impact of ipCSI. In addition, we have derived the exact expressions for OP with randomly deployed users, the accurate Monte-Carlo simulations verified the tightness of which. Thereby, the results demonstrated the performance of STAR-RIS-NOMA networks would be enhanced when increasing the number of elements of STAR-RIS. Moreover, the influence of ipCSI level was investigated in order to obtain tolerable outage performance while meeting fairness in the STAR-RIS-NOMA network under consideration. Our findings imply that the OP may be successfully sub-optimized by adjusting the power allocation parameter.

Author Contributions

H.T.T developed the system model. L.A.T and V.D.P. performed the analytic calculations and the numerical simulations while N.Q.S and Rupak Kharel wrote the whole paper. All authors contributed to the final version of the manuscript.

References

[1] Nguyen, H., T. N. Nguyen, B. V. Minh, T. -H. T. Pham, A. -T. Le and M. Voznak. Security-Reliability Analysis in CR-NOMA IoT Network Under I/Q Imbalance. *IEEE Access*. 2023, vol. 11, pp. 119045-119056. DOI: 10.1109/ACCESS.2023.3327789.

[2] Le, A. -T. et al. Power Beacon and NOMA-Assisted Cooperative IoT Networks With Co-Channel Interference: Performance Analysis and Deep Learning Evaluation. *IEEE Transactions on Mobile Computing*. 2024, vol. 23, no. 6, pp. 7270-7283. DOI: 10.1109/TMC.2023.3333764.

[3] Yang, P., Y. Xiao, M. Xiao and S. Li. 6G Wireless Communications: Vision and Potential Techniques. *IEEE Network*. 2019, vol. 33, no. 4, pp. 70-75. DOI: 10.1109/MNET.2019.1800418.

[4] Zhang, Z. et al. 6G Wireless Networks: Vision, Requirements, Architecture, and Key Technologies. *IEEE Vehicular Technology Magazine*. 2019, vol. 14, no. 3, pp. 28-41. DOI: 10.1109/MVT.2019.2921208.

[5] Phu, T. T. et al. Performance enhancement for full-duplex relaying with time-switching-based SWIPT in wireless sensors networks. *Sensors*. 2021, vol. 21, no. 11, pp. 3847. DOI: 10.3390/s21113847.

[6] Nguyen, T. N. et al. Outage Performance of Satellite Terrestrial Full-Duplex Relaying Networks With co-Channel Interference. *IEEE Wireless Communications Letters*. 2022, vol. 11, no. 7, pp. 1478-1482. DOI: 10.1109/LWC.2022.3175734.

[7] Nguyen, T. N., T. T. Duy, P. T. Tran, M. Voznak, X. Li and H. V. Poor. Partial and Full Relay Selection Algorithms for AF Multi-Relay Full-Duplex Networks With Self-Energy Recycling in Non-Identically Distributed Fading Channels. *IEEE Transactions on Vehicular Technology*. 2022, vol. 71, no. 6, pp. 6173-6188. DOI: 10.1109/TVT.2022.3158340.

[8] Nguyen, T. N. et al. On the Dilemma of Reliability or Security in Unmanned Aerial Vehicle Communications Assisted by Energy Harvesting Relaying. *IEEE Journal on Selected Areas in Communications*. 2024, vol. 42, no. 1, pp. 52-67. DOI: 10.1109/JSAC.2023.3322756.

[9] Renzo, M. D. et al. Smart radio environments empowered by reconfigurable intelligent surfaces: How it works, state of research, and the road ahead. *IEEE Journal on Selected Areas in Communications*. 2020, vol. 38, no. 11, pp. 2450-2525. DOI: 10.1109/JSAC.2020.3007211.

[10] Phan, V. -D., et al. Performance of Cooperative Communication System With Multiple Reconfigurable Intelligent Surfaces Over Nakagami-m Fading Channels. *IEEE Access*. 2022, vol. 10, pp. 9806-9816. DOI: 10.1109/ACCESS.2022.3144364.

[11] Nguyen, B. C. et al. Cooperative Communications for Improving the Performance of Bidirectional Full-Duplex System With Multiple Reconfigurable Intelligent Surfaces. *IEEE Access*. 2021, vol. 9, pp. 134733-134742. DOI: 10.1109/ACCESS.2021.3114713.

[12] Le, A. -T. et al. Performance Analysis of RIS-Assisted Ambient Backscatter Communication Systems. *IEEE Wireless Communications Letters*. 2024, vol. 13, no. 3, pp. 791-795. DOI: 10.1109/LWC.2023.3344113.

[13] Le, A. -T. et al. Physical layer security analysis for RIS-aided NOMA systems with non-colluding eavesdroppers. *Computer Communications*. 2024, vol. 219, pp. 194-203. DOI: 10.1016/j.comcom.2024.03.011.

[14] Mu, X., Y. Liu, L. Guo, J. Lin and R. Schober. Simultaneously Transmitting and Reflecting (STAR) RIS Aided Wireless Communications. *IEEE Transactions on Wireless Communications*. 2022, vol. 21, no. 5, pp. 3083-3098. DOI: 10.1109/TWC.2021.3118225.

[15] Zhang, H. et al. Intelligent Omni-Surfaces for Full-Dimensional Wireless Communications: Principles, Technology, and Implementation. *IEEE Communications Magazine*. 2022, vol. 60, no. 2, pp. 39-45. DOI: 10.1109/MCOM.001.201097.

[16] Singh, U., H. Al-Tous, O. Tirkonnen and M. R. Bhatnagar. Performance Analysis of the STAR-RIS-Assisted Downlink NOMA Communication System With MRC. *IEEE Communications Letters*. 2023, vol. 27, no. 7, pp. 1739-1743. DOI: 10.1109/LCOMM.2023.3273313.

[17] Ding, Z., X. Lei, G. K. Karagiannidis, R. Schober, J. Yuan and V. K. Bhargava. A Survey on Non-Orthogonal Multiple Access for 5G Networks: Research Challenges and Future Trends. *IEEE Journal on Selected Areas in Communications*. 2017, vol. 35, no. 10, pp. 2181-2195. DOI: 10.1109/JSAC.2017.2725519.

[18] Do, D. -T., A. -T. Le and B. M. Lee. NOMA in Cooperative Underlay Cognitive Radio Networks Under Imperfect SIC. *IEEE Access*. 2020, vol. 8, pp. 86180-86195. DOI: 10.1109/ACCESS.2020.2992660.

[19] Do, D. -T., A. -T. Le. NOMA based cognitive relaying: Transceiver hardware impairments, relay selection policies and outage performance comparison. *Computer Communications*. 2019, Vol. 146, pp. 144-154. DOI: 10.1016/j.comcom.2019.07.023.

[20] Liu, Y., Z. Qin, M. Elkashlan, Z. Ding, A. Nallanathan, and L. Hanzo. Nonorthogonal multiple access for 5G and beyond. *Proc. IEEE*. 2017, vol. 105, no. 12, pp. 2347–2381. DOI: 10.1109/JPROC.2017.2768666.

[21] Liu, Y., X. Mu, X. Liu, M. Di Renzo, Z. Ding, and R. Schober. Reconfigurable intelligent surface-aided multi-user networks: Interplay between NOMA and RIS. *IEEE Wireless Communications*. 2022, vol. 29, no. 2, pp. 169-176. DOI: 10.1109/MWC.102.2100363.

[22] Zhao, B., C. Zhang, W. Yi, and Y. Liu. Ergodic rate analysis of STAR-RIS aided NOMA systems. *IEEE Communications Letters*. 2022, vol. 26, no. 10, pp. 2297-2301. DOI: 10.1109/LCOMM.2022.3194363.

[23] Chen, J. and X. Yu. Ergodic rate analysis and phase design of STARRIS aided NOMA with statistical CSI. *IEEE Communications Letters*. 2022, vol. 26, no. 12, pp. 2889-2893. DOI: 10.1109/LCOMM.2022.3202346.

[24] Gunasinghe, D. and G. Amarasuriya. Performance Analysis of STAR-RIS for Wireless Communication. In:*ICC 2022 - IEEE International Conference on Communications*. Seoul, Republic of Korea, 2022, pp. 3275-3280. DOI: 10.1109/ICC45855.2022.9838939.

[25] Yue, X., J. Xie, Y. Liu, Z. Han, R. Liu and Z. Ding. Simultaneously Transmitting and Reflecting Reconfigurable Intelligent Surface Assisted NOMA Networks. *IEEE Transactions on Wireless Communications*. 2023, vol. 22, no. 1, pp. 189-204. DOI: 10.1109/TWC.2022.3192211.

[26] Aldababsa, M., A. Khaleel, and E. Basar. Simultaneous transmitting and ReflectingIntelligent surfaces-empowered NOMA networks. 2021. DOI: 10.48550/arXiv.2110.05311.

[27] Wang, T., M.-A. Badiu, G. Chen, and J. P. Coon. Outage probability analysis of STAR-RIS assisted NOMA network with correlated channels. *IEEE Communications Letters*. 2022 vol. 26, no. 8, pp. 1774-1778. DOI: 10.1109/LCOMM.2022.3174453.

[28] Chauhan, A., S. Ghosh and A. Jaiswal. RIS Partition-Assisted Non-Orthogonal Multiple Access (NOMA) and Quadrature-NOMA With Imperfect SIC. *IEEE Transactions on Wireless Communications*. 2023, vol. 22, no. 7, pp. 4371-4386. DOI: 10.1109/TWC.2022.3224645.

[29] Xie, K., G. Cai, G. Kaddoum and J. He. Performance Analysis and Resource Allocation of STAR-RIS-Aided Wireless-Powered NOMA System. *IEEE Transactions on Communications*. 2023, vol. 71, no. 10, pp. 5740-5755. DOI: 10.1109/TCOMM.2023.3292471.

[30] Mahmoud, A., A. A. Mwais, and M. Obaid. Performance of STAR-RIS assisted NOMA networks in Nakagami-m fading channels. *AEU-International Journal of Electronics and*

Communications. 2023, vol. 166 pp. 154685. DOI: 10.1016/j.aeue.2023.154685.

[31] Li, Q. et al. Achievable Rate Analysis of the STAR-RIS-Aided NOMA Uplink in the Face of Imperfect CSI and Hardware Impairments. *IEEE Transactions on Communications*. 2023, vol. 71, no. 10, pp. 6100-6114. DOI: 10.1109/TCOMM.2023.3287995.

[32] Andrews, J. G., R. K. Ganti, M. Haenggi, N. Jindal and S. Weber. A primer on spatial modeling and analysis in wireless networks, *IEEE Commun. Mag.*. 2010, vol. 48, iss. 11, pp. 156-163. ISSN 0163-6804 DOI: 10.1109/MCOM.2010.5621983.

[33] Alexis I. Aravanis et. al, . A tractable closed form approximation of the ergodic rate in Poisson cellular networks, *EURASIP Journal on Wireless Communications and Networking*. 2019, Art.no.187. DOI: 10.1186/s13638-019-1499-9.

[34] B. Zhao, C. Zhang, W. Yi, and Y. Liu, Ergodic rate analysis of star-ris aided noma systems. *IEEE Communications Letters*. 2022, vol. 26, iss. 10, pp. 2297-2301. ISSN: 1089-7798. DOI: 10.1109/LCOMM.2022.3194363.

[35] Le, C. -B., D. -T. Do, X. Li, Y. -F. Huang, H. -C. Chen and M. Voznak. Enabling NOMA in backscatter reconfigurable intelligent surfaces-aided systems. *IEEE Access*. 2021, vol. 9, pp. 33782-33795. ISSN 2169-3536. DOI: 10.1109/ACCESS.2021.3061429.

[36] Nguyen, T. N., et al. Performance analysis of a user selection protocol in cooperative networks with power splitting protocol-based energy harvesting over Nakagami-m/Rayleigh channels. *Electronics*. 2019, vol. 8, no. 9 pp. 448. DOI: 10.3390/electronics8040448.

[37] Nguyen, T. N., et al. Multisource power splitting energy harvesting relaying network in half-duplex system over block Rayleigh fading channel: System performance analysis. *Electronics*. 2019, vol. 8, no. 1 pp. 67. DOI: 10.3390/electronics8010067.

[38] Nguyen, T. N., et al. Outage Probability Analysis for Relay-Aided Self-Energy Recycling Wireless Sensor Networks Over INID Rayleigh Fading Channels. *IEEE Sensors Journal*. 2024, vol. 24, no. 7, pp. 11184-11194. DOI: 10.1109/JSEN.2024.3365698.

[39] Gradshteyn, I.S and Ryzhik, I.M. *Table of integrals, series, and products*. Elsevier/Academic Press, 2007.

[40] Phan, V. -D., et al. A study of physical layer security in SWIPT-based decode-and-forward relay networks with dynamic power splitting. *Sensors*. 2021, vol. 21, no. 17, pp. 5692. DOI: 10.3390/s21175692.

[41] Tu, L. -T., et al. Broadcasting in cognitive radio networks: A fountain codes approach. *IEEE Transactions on Vehicular Technology*. 2022, vol. 71, no. 10, pp. 11289-11294. DOI: 10.1109/TVT.2022.3188969.

[42] Phan, V. D., et al. Reliability-Security in Wireless-Powered Cooperative Network with Friendly Jammer. *Advances in Electrical and Electronic Engineering*. 2023, vol. 20, no. 4, pp. 584-591. DOI: 10.15598/aeee.v20i4.4511.

[43] Nguyen, T. N., et al. Performance evaluation of user selection protocols in random networks with energy harvesting and hardware impairments. *Advances in Electrical and Electronic Engineering*. 2016, vol. 14, no. 4, pp. 372-377. DOI: 10.15598/aeee.v14i4.1783.

[44] Do, D. -T., A. -T. Le, Y. Liu and A. Jamalipour. User Grouping and Energy Harvesting in UAV-NOMA System With AF/DF Relaying. *IEEE Transactions on Vehicular Technology*. 2021, vol. 70, no. 11, pp. 11855-11868. DOI: 10.1109/TVT.2021.3116101.

[45] Huynh, T. P., P. N. Son, and M. Voznak. Exact Throughput Analyses of Energy-Harvesting Cooperation Scheme with Best Relay Selections Under I/Q Imbalance. *Advances in Electrical and Electronic Engineering*. 2017, vol. 15, no. 4, pp. 585-590. DOI: 10.15598/aeee.v15i4.2302.

[46] Bui V.M., A.V. LE, V.D. PHAN, T.H.T. PHAM. Self-Energy Recycling in DF Full-Duplex Relay Network: Security-Reliability Analysis. *Advances in Electrical and Electronic Engineering*. 2024, vol. 22, no. 1, pp. 86-96. DOI: 10.15598/aeee.v22i1.5528.

[47] Nguyen, T. N., et al. Performance enhancement for energy harvesting based two-way relay protocols in wireless ad-hoc networks with partial and full relay selection methods. *Ad hoc networks*. 2019, vol. 84, pp. 178-187. DOI: 10.1016/j.adhoc.2018.10.005.

[48] NGUYEN, T. N., et al. Energy harvesting over Rician fading channel: a performance analysis for half-duplex bidirectional sensor networks under hardware impairments. *Sensors*, 2018, vol. 18, no. 6, pp. 1781. DOI: 10.3390/s18061781.

[49] MINH, B. V., et al. D2D Communication Network with the Assistance of Power Beacon under the Impact of Co-channel Interferences and Eavesdropper: Performance Analysis. *Advances in Electrical and Electronic Engineering*, 2024, vol. 21, no. 4, pp. 351-359. DOI: 10.15598/aeee.v21i4.5495.

[50] HOANG, T, M,, et al. Performance and optimal analysis of time-switching energy harvesting protocol for MIMO full-duplex decode-and-forward wireless relay networks with various transmitter and receiver diversity techniques. *Journal of the Franklin Institute*, 2020, vol. 357, no. 17, pp. 13205-13230. DOI: 10.1016/j.jfranklin.2020.09.037.

[51] DUNG, C. T., et al. Secrecy performance of multi-user multi-hop cluster-based network with joint relay and jammer selection under imperfect channel state information. *Performance Evaluation*, 2021, vol. 147, pp. 102193. DOI: 10.1016/j.peva.2021.102193.

[52] Do, T. N., G. Kaddoum, T. L. Nguyen, D. B. da Costa and Z. J. Haas. Multi-RIS-aided wireless systems: Statistical characterization and performance analysis. *IEEE Trans. Commun.*. 2021, vol. 69, iss. 12, pp. 8641-8658. ISSN: 0090-6778. DOI: 10.1109/TCOMM.2021.3117599.

[53] ABRAMOWITZ, M. and STEGUN, I. A. *Handbook of Mathematical Functions with Formulas, Graphs, and Mathematical Tables.* New York, NY, USA: Dover, 1972.

About Authors (Optional)

Sang Quang NGUYEN received the BE degree (2010) and M.E. degree (2013) in Ho Chi Minh City University of Transport and Ho Chi Minh City University of Technology, Vietnam, respectively. In 2017, he received the Ph.D. degree in Electrical Engineering from University of Ulsan, South Korea. His major research interests are cooperative communications, cognitive radio, physical layer security, combining techniques. Since January - June 2017, he was a post-doc research fellow at Queen's University Belfast. His major research interests are: Cooperative communication, Cognitive radio, Physical layer security, Energy harvesting, Non-orthogonal multiple access, Unreliable backhaul connections.

Anh-Tu LE was born in Lam Dong, Vietnam, in 1997. He received the B.S. degree from the Industrial University of Ho Chi Minh City, Vietnam, in 2019, and the M.S. degree from Ton Duc Thang University, Vietnam, in 2022. He has authored and co-authored over 25 ISI-indexed journals. His research interests include wireless channel modeling, NOMA, cognitive radio, MIMO, and machine learning.

Van-Duc PHAN was born in 1975 in Long An province, Vietnam. He received his M.S. degree in Department of Electric, Electrical and Telecommunication Engineering from Ho Chi Minh City University of Transport, Vietnam and Ph.D. degree in Department of Mechanical and Automation Engineering, Da-Yeh University, Taiwan in 2016. Currently, his research interests are in sliding mode control, nonlinear systems or active magnetic bearing, flywheel store energy systems, power system optimization, optimization algorithms, and renewable energies, Energy harvesting (EH) enabled cooperative networks, Improving the optical properties, lighting performance of white LEDs, Energy efficiency LED driver integrated circuits, Novel radio access technologies, Physical security in communication network.

Huynh Thanh THIEN (corresponding author) received the Ph.D. degree in electrical and computer engineering from the University of Ulsan, Ulsan, South Korea. He is working as a lecturer at the Faculty of Electrical and Electronics Engineering, Ton Duc Thang University, Ho Chi Minh City, Vietnam. His research interests include cognitive radio and next-generation wireless communications systems, game theory, deep learning, reinforcement learning, and semiconductor device.

Rupak KHAREL received the Ph.D. degree in secure communication systems from Northumbria University, U.K., in 2011. He is currently the Associate Dean and a Professor with the School of Computing and Engineering, University of Huddersfield. He is a principal investigator of multiple government and industry-funded research projects. His research interests include various use cases and the challenges of the IoT and cyber-physical systems (CPS), cyber security challenges on CPS, the energy optimization of the IoT networks for green computing, the Internet of connected Vehicles (IoV), and smart infrastructure systems. He is a member of the IET and a fellow of the Higher Education Academy (FHEA), U.K.or networks, 5G, and Industry 4.0.

Appendix A Proof of Theorem 1

Substituting (1a) and (9a) into (10), $\mathcal{O}_1$ is expressed as

$$\begin{aligned}\mathcal{O}_1 =&1-\Pr\left(|A_1|^2>\psi_{\max}\left(\rho_S\sigma_{e_1}^2+d_0^\alpha d_1^\alpha\right)\right)\\ =&1-\int_0^{R_1} f_{d_{U_1}}(x)\left[1-F_{|A_1|^2}\left(\psi_{\max}\left(\rho_S\sigma_{e_1}^2+d_0^\alpha x^\alpha\right)\right)\right]dx\\ =&1-\frac{4\psi_{\max}^{\frac{N}{2}}}{R_1^2\Gamma(N)\left(\sqrt{\lambda_{h_0}\lambda_{h_1}}\right)^N}\int_0^{R_1} x\left(\rho_S\sigma_{e_1}^2+d_0^\alpha x^\alpha\right)^{\frac{N}{2}}\\ &\times K_N\left(2\sqrt{\frac{\psi_{\max}\left(\rho_S\sigma_{e_1}^2+d_0^\alpha x^\alpha\right)}{\lambda_{h_0}\lambda_{h_1}}}\right)dx.\end{aligned}\tag{18}$$

Let $t=\frac{2x}{R_1}-1\to\frac{R_1(t+1)}{2}=x\to\frac{R_1}{2}dt=dx$, $\mathcal{O}_1$ is calculated as

$$\begin{aligned}\mathcal{O}_1 =&1-\frac{2\psi_{\max}^{\frac{N}{2}}}{R_1\Gamma(N)\left(\sqrt{\lambda_{h_0}\lambda_{h_1}}\right)^N}\int_{-1}^{1}\Phi(t)\left(\rho_S\sigma_{e_1}^2+d_0^\alpha\Phi(t)^\alpha\right)^{\frac{N}{2}}\\ &\times K_N\left(2\sqrt{\frac{\psi_{\max}\left(\rho_S\sigma_{e_1}^2+d_0^\alpha\Phi(t)^\alpha\right)}{\lambda_{h_0}\lambda_{h_1}}}\right)dt,\end{aligned}\tag{19}$$

where $\Phi(t)=\frac{R_1(t+1)}{2}$.

Although obtaining a closed-form formula for $\mathcal{O}_1$ is challenging, we can acquire an accurate approximation for it. Using the Gaussian-Chebyshev quadrature [53, Eq. (25.4.38)], (11) can be obtained. The proof is complete.

Appendix B Proof of Theorem 2

Similar to (18), (12) can be rewritten as

$$\begin{aligned}&\mathcal{O}_2=1-\Pr\left(|A_2|^2>\psi_2\left(\rho_S\sigma_{e_2}^2+d_0^\alpha d_2^\alpha\right)\right)\\ &=1-\int_{R_1}^{R_2} f_{d_{U_2}}(x)\left[1-F_{|A_2|^2}\left(\psi_2\left(\rho_S\sigma_{e_2}^2+d_0^\alpha x^\alpha\right)\right)\right]dx\\ &=1-\frac{4\psi_2^{\frac{N}{2}}}{\left(R_2^2-R_1^2\right)\Gamma(N)\left(\sqrt{\lambda_{h_0}\lambda_{h_2}}\right)^N}\int_{R_1}^{R_2} x\left(\rho_S\sigma_{e_2}^2+d_0^\alpha x^\alpha\right)^{\frac{N}{2}}\\ &\times K_N\left(2\sqrt{\frac{\psi_2\left(\rho_S\sigma_{e_2}^2+d_0^\alpha x^\alpha\right)}{\lambda_{h_0}\lambda_{h_2}}}\right)dx.\end{aligned}\tag{20}$$

Let $t=\frac{2x-R_1-R_2}{R_2-R_1}\to\left(\frac{R_2+R_1}{2}\right)+\left(\frac{R_2-R_1}{2}\right)t=x\to\left(\frac{R_2-R_1}{2}\right)dt=dx$, $\mathcal{O}_2$ can be derived as

$$\begin{aligned}\mathcal{O}_2 =&1-\frac{2\left(R_2-R_1\right)\psi_2^{\frac{N}{2}}}{\left(R_2^2-R_1^2\right)\Gamma(N)\left(\sqrt{\lambda_{h_0}\lambda_{h_2}}\right)^N}\\ &\times\int_{-1}^{1}\Delta(t)\left(\rho_S\sigma_{e_2}^2+d_0^\alpha\Delta(t)^\alpha\right)^{\frac{N}{2}}\\ &\times K_N\left(2\sqrt{\frac{\psi_2\left(\rho_S\sigma_{e_2}^2+d_0^\alpha\Delta(t)^\alpha\right)}{\lambda_{h_0}\lambda_{h_2}}}\right)dt,\end{aligned}\tag{21}$$

where $\Delta(t)=\left(\frac{R_2+R_1}{2}\right)+\left(\frac{R_2-R_1}{2}\right)t$. Finally, we employ the Chebyshev-Gauss-quadrature to obtain (13). This proof is complete.